A Comparison of Numerical Schemes for Convection on a Fourth-Order Diffusion Equation

by

Youngsoo Ha, Yong-Jung Kim, and Tim G. Myers

Applied Mathematics
Research Report
07-03
July 30, 2007

DEPARTMENT OF MATHEMATICAL SCIENCES

KAIST 한국과학기술원
Korea Advanced Institute of Science and Technology

A comparison of numerical schemes for convection on a fourth-order diffusion equation

Youngsoo Ha [a] , Yong-Jung Kim [a]

[a] *Department of Mathematical Sciences, KAIST (Korea Advanced Institute of Science and Technology), 373-1 Gusong-dong, Yusong-gu, Taejon, 305-701, South Korea*

Tim G. Myers [b]

[b] *Department of Mathematics & Applied Mathematics, University of Cape Town, South Africa*

Abstract

This paper is devoted to comparing numerical schemes for a differential equation with convection and fourth-order diffusion. Our model equation is $u_t + (u^2 - u^3)_x = -(u^3 u_{xxx})_x$, which arises in the context of thin film flow. First we employ implicit schemes and treat both convection and diffusion terms simultaneously. Then the convection terms are treated with well-known explicit schemes, namely Godunov, WENO and central-upwind, while the diffusion term is treated implicitly. The diffusion and convection schemes are combined using a fractional step splitting method.

1 Introduction

In this paper we consider numerical solutions to the following equation

$$u_t + f(u)_x = -(u^3 u_{xxx})_x, \tag{1.1}$$

Email addresses: young@amath.kaist.ac.kr (Youngsoo Ha), yongkim@kaist.edu (Yong-Jung Kim), myers@maths.uct.ac.za (Tim G. Myers).

where the flux is given by

$$f(u) = u^2 - u^3. \tag{1.2}$$

Equation (1.1) describes the flow of a thin liquid film, where $u(x,t) \geq 0$ denotes the film thickness. The flux terms represent surface shear and gravity, where the forces act in opposing directions, the diffusion term on the right hand side represents surface tension. The surface shear term may arise due to temperature or concentration gradients or to an external shear force (caused by wind for example). Derivations of equation (1.1) and related equations may be found in the reviews [19,23]. For the specific case when thermocapillary effects produce the surface shear, equation (1.1) is derived in [10,3], with a wind induced stress a derivation is given in [20,21]. Experimental results showing typical film shapes for thermocapillary flow up a vertical plate are presented in [10].

The numerical solution of equations (1.1, 1.2) is constrained by the diffusion term. An explicit scheme requires a time-step Δt of the order $(\Delta x)^4$. Consequently in regions where high resolution is required, such as at a moving front, a singularity or at blow-up, the computational time is prohibitive. Implicit methods are therefore generally preferred. Recently these have been coupled with adaptive meshes to permit high accuracy in the regions of primary interest, see [24,12,2,30] for example. However, the first-order convection term is not subject to the same constraint and there are many different methods to deal with nonlinear convection. In the following work we focus primarily on a comparison between finite difference, Godunov, central-upwind and WENO schemes applied to the convection term. We also investigate the effect of applying fully implicit and Crank-Nicolson schemes. Fractional step splitting,

alternating between solving for the diffusion and convection terms, is applied in all cases since this was shown in our early numerical simulations to be significantly more stable than solving the full equation in a single step.

The majority of our numerical examples will be taken from [3]. We use these examples because Bertozzi *et al* [3] present a very careful numerical and analytical investigation of equations (1.1, 1.2) and the cases presented show a wide variety of behaviour in the solutions. The flux function has a point of inflexion at $u = 1/3$. The form of solution is likely to change around this point, consequently in our numerical solutions we will take limiting values for u close to this value.

2 Numerical Schemes

The notation employed in the numerical calculations is as follows. We consider a uniform mesh $x_{j+1/2}$ with a fixed width $h \equiv \Delta x > 0$, where $x_{j+1/2} = (j+1/2)h$, $j \in \mathbf{Z}$. The time mesh is given by $t^n = n\Delta t$, with a fixed time step size $\Delta t > 0$. We write U_j^n as the approximation to the cell average of the true solution, i.e.,

$$U_j^n \simeq \frac{1}{h} \int_{x_{j-1/2}}^{x_{j+1/2}} u(x, t^n) dx \ . \tag{2.1}$$

The diffusion term in equation (1.1) will be tackled via an implicit finite difference scheme. The convection term will be dealt with via the implicit and and various explicit methods. The diffusion and convection schemes will be combined using a fractional step splitting method.

First we consider a finite difference scheme for the diffusion equation

$$u_t = -(u^3 u_{xxx})_x \ . \tag{2.2}$$

Since

$$u(x+2h) - 2u(x+h) + 2u(x-h) - u(x-2h) = 2h^3 u_{xxx}(x) + O(h^5) \ ,$$

we obtain the following finite difference representation

$$(u^3 u_{xxx})_j \cong \frac{(U_j^n)^3}{2h^3}(U_{j+2}^n - 2U_{j+1}^n + 2U_{j-1}^n - U_{j-2}^n) \equiv \frac{\Phi(U^n; j)}{2h^3} \ .$$

Then the fourth order diffusion equation (2.2) may be discretized as

$$\begin{aligned} U_j^{n+1} = U_j^n - \tfrac{\Delta t}{4h^4}\Big[\ & \theta\Big(\Phi(U^{n+1}; j+1) - \Phi(U^{n+1}, j-1)\Big) \\ & +(1-\theta)\Big(\Phi(U^n, j+1) - \Phi(U^n; j-1)\Big)\Big], \end{aligned} \tag{2.3}$$

where θ is a weighting factor. If $\theta = 0.5$, then the method is Crank-Nicolson (denoted CN from now on), with second order accuracy in space and time. If $\theta = 1$ then the method is fully implicit (denoted FI), with first order in time and second order in space.

The convection equation

$$u_t = -f(u)_x \tag{2.4}$$

can also be solved using a finite difference scheme. This has the advantage of simplicity, in that all terms in the full governing equation can be dealt with in the same manner. The finite difference discretization of equation (2.4) is

given by

$$U_j^{n+1} = U_j^n - \frac{\Delta t}{2h}\Big[\theta\Big(f(U_{j+1}^{n+1}) - f(U_{j-1}^{n+1})\Big) + (1-\theta)\Big(f(U_{j+1}^{n}) - f(U_{j-1}^{n})\Big)\Big].$$

2.2 Alternative schemes for the convection equation

Many schemes have been developed and are widely used to deal with convection. We will now investigate the application of Godunov, central-upwind (CU) and WENO methods to the flux term of equation (1.2).

We view $u_{j+1/2}^n$ as an approximation of $u(x,t)$ at the interface $x_{j+1/2}$ of each cell. In a conservative numerical scheme the flux at the interface is approximated using its neighbouring cell averages and we set

$$f(u_{j+1/2}^n) \equiv F(U^n; j) \sim f(u(x_{j+1/2}, t)), \qquad t^n \le t \le t^{n+1}\ , \tag{2.5}$$

where F denotes the cell average flux.

Then, after integrating (2.4) over the mesh $[x_{j-1/2}, x_{j+1/2}] \times [t^n, t^{n+1}]$, one obtains

$$U_j^{n+1} = U_j^n - \frac{\Delta t}{h}(f(u_{j+1/2}^n) - f(u_{j-1/2}^n))\ . \tag{2.6}$$

The choice of numerical scheme determines the form of the flux function in equation (2.6).

2.2.1 Godunov scheme

Godunov schemes [5,15,28] are based on either the exact or an approximate solution of the Riemann problem using characteristic information within the

framework of a conservative method. Since the Godunov method can be written in conservative form with a proper CFL condition, we can find:

$$U_j^{n+1} = U_j^n - \frac{\Delta t}{h}\left(\max(s_{j-1/2}^n, 0)(U_j^n - U_{j-1}^n) + \min(s_{j+1/2}^n, 0)(U_{j+1}^n - U_j^n)\right).$$

Here, $s_{j+1/2}^n$ is the shock speed at the interface $x_{j+1/2}$ determined by the Rankine-Hugoniot jump condition,

$$s_{j+1/2}^n = [f(U_{j+1}^n) - f(U_j^n)]/(U_{j+1}^n - U_j^n)\ . \tag{2.7}$$

The Godunov method can be modified to a second order scheme by employing proper limiters. For the present study we use CLAWPACK [17] with either a monotonized centered (MC), van Leer (VL) or Superbee (SB) limiter.

2.2.2 Central-upwind (CU) scheme

A Godunov-type semi-discrete central scheme was introduced in [13,14]. We first compute the local speeds of propagation at the interface $x = x_{j+1/2}$. Since the speed of propagation is related to the CFL condition, we can estimate the local speeds of the right and left side of the cell boundary. The local speeds of wave propagation are bounded by $s_{j+1/2,r}^n$ and $s_{j+1/2,l}^n$ which are given by

$$s_{j+1/2,r}^n = \max_{\mathcal{C}}(f'(u), 0) \qquad\qquad s_{j+1/2,l}^n = \min_{\mathcal{C}}(f'(u), 0)\ , \tag{2.8}$$

where $\mathcal{C}$ is a relevant range for h. Employing this local speed of propagation the flux at the interface is approximated by

$$f(u_{j+1/2}^n) = \frac{s_{j+1/2,r} f(u_{j+1/2}^-) - s_{j+1/2,l} f(u_{j+1/2}^+)}{s_{j+1/2,r} - s_{j+1/2,l}} + \frac{s_{j+1/2,r} s_{j+1/2,l}}{s_{j+1/2,r} - s_{j+1/2,l}}[u_{j+1/2}^+ - u_{j+1/2}^-]\ , \tag{2.9}$$

where $u^+_{j+1/2}$ and $u^-_{j+1/2}$ are computed as

$$u^+_{j+1/2} \equiv U^n_{j+1} - \frac{h}{2}(u_x)_{j+1}(t^n) \qquad u^-_{j+1/2} \equiv U^n_j + \frac{h}{2}(u_x)_j(t^n),$$

$$(u_x)_j = \text{minmod}(\alpha\frac{U^n_{j+1} - U^n_j}{h}, \frac{U^n_{j+1} - U^n_{j-1}}{h}, \alpha\frac{U^n_j - U^n_{j-1}}{h}) \ , \quad 1 \le \alpha \le 2 \ .$$

The effect of changing α is discussed in subsequent sections. In general we should use $\alpha \in [1, 2]$ but we find that when $\alpha \le 1.1$ the solution rapidly moves out of the computational domain.

2.2.3 WENO method

The weighted essentially non-oscillatory (or WENO) method is described in [7,6,9,18,25]. The ENO method has been combined with an adaptive mesh code in a study of the stability of moving contact lines in [12]. Greer *et al* [4] compare a fifth order WENO and upwind schemes in a study of fourth-order partial differential equations on an arbitrary surface. They conclude that the requirements of accuracy and efficiency suggest that WENO is preferable to the other schemes.

To avoid entropy violating solutions and obtain numerical stability we split the flux $f(u)$ into two components f^+ and f^- such that

$$f(u) = f^+(u) + f^-(u) \ , \tag{2.10}$$

where $f^+_u \ge 0$ and $f^-_u \le 0$. One of the simplest flux splitting methods is Lax-Friedrichs splitting, which is given by

$$f^\pm(u) = \frac{1}{2}(f(u) \pm \gamma u) \ , \tag{2.11}$$

where $\gamma = \max_u |f'(u)|$ over the pertinent range of u which can be decided *a priori*. The interface approximation of the fifth order WENO with Lax-Friedrichs splitting (WENO-LF**5** for short) is given by

$$\begin{aligned} f(u^n_{j+1/2}) = & \frac{1}{12}(-f_{j-1} + 7f_j + 7f_{j+1} - f_{j+2}) - \\ & \Phi_N(\Delta f^+_{j-\frac{3}{2}}, \Delta f^+_{j-\frac{1}{2}}, \Delta f^+_{j+\frac{1}{2}}, \Delta f^+_{j+\frac{3}{2}}) + \Phi_N(\Delta f^-_{j+\frac{5}{2}}, \Delta f^-_{j+\frac{3}{2}}, \Delta f^-_{j+\frac{1}{2}}, \Delta f^-_{j-\frac{1}{2}}) \ , \end{aligned}$$

where $f_j = f(u^n_j)$, $f^\pm_j = f^\pm(u^n_j)$, $\Delta f^\pm_{i+\frac{1}{2}} = f^\pm_{i+1} - f^\pm_i$ and

$$\Phi_N(a,b,c,d) = \frac{1}{3}\omega_0(a - 2b + c) + \frac{1}{6}(\omega_2 - \frac{1}{2})(b - 2c + d) \ . \tag{2.12}$$

The nonlinear weights ω_0 and ω_2 are defined by

$$\omega_j = \frac{\gamma_j}{\sum_{l=0}^{k-1} \gamma_l} \ , \quad \gamma_l = \frac{d_l}{(\varepsilon + \beta_l)^2} \ , \quad d_0 = \frac{1}{10} \ , \quad d_1 = \frac{3}{5} \ , \quad d_2 = \frac{3}{10} \ ,$$

where, in this case, $k = 3$ and $0 < \varepsilon \ll 1$ is introduced to prevent singularity and the smoothness indicators β_j's are given by

$$\begin{aligned} \beta_0 &= \tfrac{13}{12}(f_{i-2} - 2f_{i-1} + f_i)^2 + \tfrac{1}{4}(f_{i-2} - 4f_{i-1} + 3f_i)^2 \\ \beta_1 &= \tfrac{13}{12}(f_{i-1} - 2f_i + f_{i+1})^2 + \tfrac{1}{4}(f_{i-1} - f_{i+1})^2 \\ \beta_2 &= \tfrac{13}{12}(f_i - 2f_{i+1} + f_{i+2})^2 + \tfrac{1}{4}(3f_i - 4f_{i+1} + f_{i+2})^2 \ . \end{aligned} \tag{2.13}$$

3 Computation of the convection terms

3.1 Linear Transport Equation

In this section we show two numerical examples for convection equations that highlight certain properties of interest to our subsequent calculations on the full problem.

Consider the linear transport equation

$$u_t + u_x = 0 \qquad\qquad u(x,0) = u_0(x)\ . \tag{3.1}$$

The exact solution of this problem is simply $u(x,t) = u_0(x-t)$. When we take sufficiently smooth initial data the numerical solutions for all the schemes introduced in §2, both implicit and explicit, provide accurate results. However, this is not the case with discontinuous data.

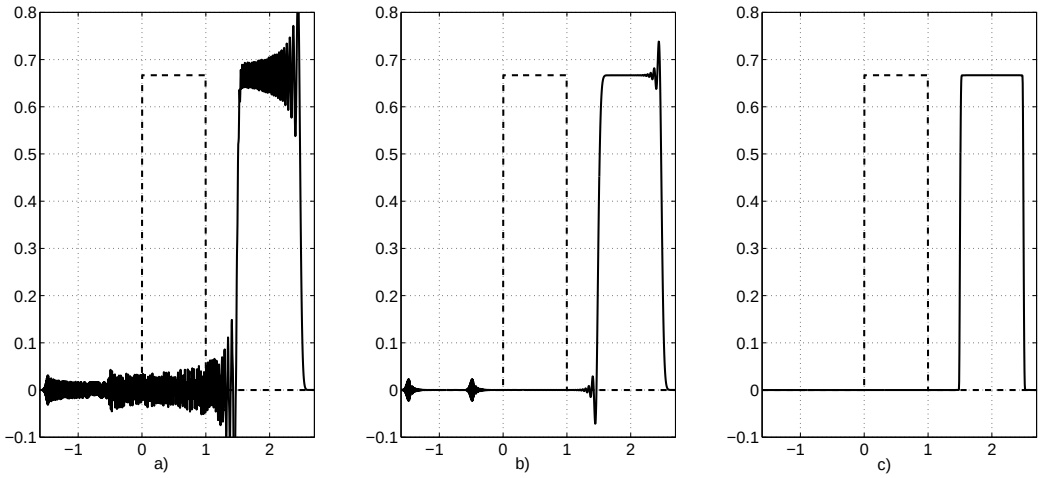

Fig. 1. Comparison of a) CN, b) FI and c) Godunov solutions with the exact solution of equation (3.1) with initial condition (3.2).

Consider the discontinuous initial profile

$$u_0(x) = \begin{cases} 2/3, & 0 < x < 1, \\ 0, & \text{otherwise.} \end{cases} \tag{3.2}$$

Numerical solutions using CN, FI and the Godunov method are shown as the solid lines on Figure 1, with $h = 0.01$ and $\Delta t = 0.03, 0.03, 0.075$ for the respective schemes. The initial condition is shown as a dashed line. The explicit scheme allows much larger time-steps than the two implicit schemes. WENO and CU are not shown, since they are indistinguishable from the Godunov results. Both implicit schemes show strong oscillations behind the

discontinuity, although CN is clearly the worst. However, if we increase the time-step to $\Delta t = 0.05$ the CN result shows little change while the FI scheme becomes unstable and we do not obtain a result.

In general the oscillatory behaviour exhibited by CN and FI schemes forces the use of smooth initial data for the thin film equation (1.1). Godunov (and WENO and CU) is designed to deal with convection equations with a possible discontinuity and consequently the solutions show no oscillations. In the numerical results of §4, where we incorporate the diffusion term, we will deal with both continuous and discontinuous initial data.

3.2 Convection with non-convex flux, $f(u) = u^2 - u^3$

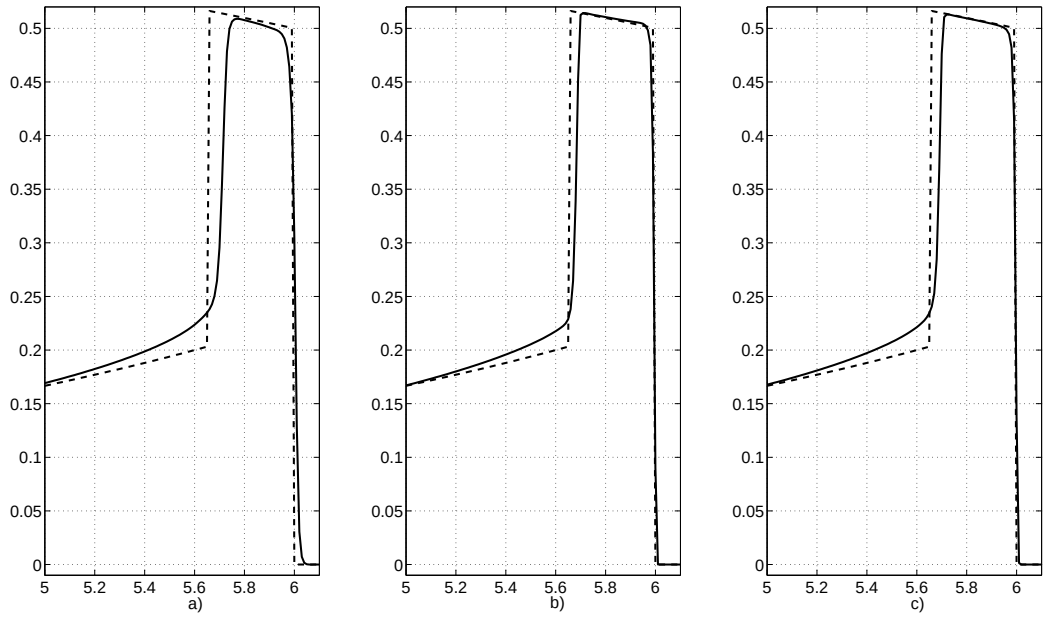

Fig. 2. Comparison of a) WENO, b) CU and c) Godunov schemes applied to equation (3.3) with discontinuous initial data (3.2). The exact solution is shown as the solid line.

Consider the conservation law, equation (1.1), with the diffusion term ne-

glected

$$u_t + f(u)_x = 0, \qquad f(u) = u^2 - u^3, \quad u(x,0) = u_0(x), \tag{3.3}$$

where the initial value is given by the discontinuous data of equation (3.2). This type of travelling wave is similar to the double shocks discussed in the following section. One can easily find the exact solution of the problem using rarefaction waves and the equal area rule [11]. This is shown as the dashed line in Figure 2. Numerical solutions are also shown in the figures using the three explicit methods (the implicit methods all show oscillations and so are neglected). Away from the discontinuity all of the numerical solutions show excellent agreement with the exact solution. However, at the downstream side of the shock the solutions diverge, with WENO showing the greatest error. Central upwind shows a slightly lower error than Godunov. On the upstream side all solutions show relatively good agreement.

The choice of CFL number is important to the explicit schemes. The aim is to accurately capture a discontinuity, without producing oscillations, while achieving a fast runtime. For a convex flux a high CFL, close to unity, is generally chosen for Godunov and CU schemes. WENO usually requires a CFL around 0.5. In this paper, we deal with a non-convex flux. Taking a CFL of 0.9 in the above example for Godunov results in oscillations. We found a CFL of 0.75 removed the oscillations while retaining a fast runtime. A similar value was satisfactory for CU, while WENO ran with good accuracy at the standard value of 0.5.

The results so far demonstrate the difficulty encountered by the implicit methods in the presence of a discontinuity. For small time-steps the fully implicit scheme shows relatively small oscillations, but large time-steps cause the so-

lution to blow up. CN tends to show significant oscillations for a large range of time-steps but did provide a solution for all the cases investigated. The three explicit methods all deal well with discontinuities, with WENO showing slightly worse agreement with the exact solution than the other two. However, to obtain satisfactory solutions the CFL number should be around 0.75 for Godunov and CU and 0.5 for WENO.

4 Computation of the full equation

Now we return to the original problem, specified by equations (1.1) and (1.2), and compare the different numerical schemes. To solve the equation numerically we employ a fractional step splitting method that alternates between solving the diffusion equation (2.2) and the convection equation (2.4). Step splitting increases the stability of the solutions to such an extent that in the following examples we will not show any solutions obtained without step-splitting. In all of the following examples when we employ an explicit scheme to the convection term, we calculate the diffusion term using the CN scheme. As will be seen later this is the most reliable of the two implicit schemes. From now on we will refer to the schemes that involve explicit methods as the explicit schemes, despite the implicit diffusion component. This is to provide a simple distinction from the CN and FI schemes.

To clearly distinguish between the different schemes and avoid differences caused by the behaviour due to the initial condition it is best to compare results at large times. Obviously this can lead to large computational domains and consequently large computation times. In most examples we therefore

modify equation (1.1) to move with the region of interest

$$u_t + f(u)_x - su_x = -(u^3 u_{xxx})_x \ , \tag{4.1}$$

where the wave speed s is defined by equation (2.7).

The addition of the new term means that we must introduce one more step to the splitting method

$$u_t = su_x \ . \tag{4.2}$$

To ensure that this part of the equation does not interfere with our investigation of the numerical schemes we compute (4.2) using the central method [22] for all cases.

4.1 Comparison of schemes for a travelling wave

Our aim in this section is to test the numerical schemes described in §2. We will do this by examining a standard thin film flow example of a travelling wave with a Lax shock. The travelling wave joins two regions of different heights, u_l and u_r, where

$$u_l = \lim_{x\to-\infty} u(x) \qquad\qquad u_r = \lim_{x\to\infty} u(x) \ .$$

In the limit $u_r \ll 1$ this can represent a thin film moving over a precursor layer. However, as pointed out in [3], any value of $0 < u_r < 1/3$ will show the same qualitative behaviour. Bertozzi *et al* [3] show that multiple Lax shocks are possible for this situation, depending on the initial conditions. As discussed earlier, both CN and FI methods have difficulties in dealing with discontinuous initial values, hence they use a continuous initial condition

involving a hyperbolic tangent. We will discuss the effect of discontinuous initial conditions in the following sections.

For comparison purposes we must first determine the travelling wave solution which obviously should propagate with no time variation. This solution will be imposed as the initial value for the numerical schemes. We may then test the accuracy of the schemes by observing how the numerical solutions diverge from the travelling wave over time. An alternative test would be to start with a smooth function, such as the hyperbolic tangent, and observe how the numerical solution tends to the travelling wave over time. However, our method allows us to make a meaningful comparison after a relatively short time and removes the problem of determining whether the error occurs because the numerical solution has not yet reached a steady-state.

To determine the travelling wave solution we start by making the substitution $\xi = x - st$ where s is the wave speed. This allows equation (1.1) to be integrated once and written as

$$u_{\xi\xi\xi} = \frac{su + u^3 - u^2 + c}{u^3} \ . \tag{4.3}$$

The far-field solutions $x \to -\infty, u \to u_l$ and $x \to \infty, u \to u_r$ allow the values of s and c to be calculated

$$s = \frac{(u_l^2 - u_l^3) - (u_r^2 - u_r^3)}{u_l - u_r} = \frac{f(u_l) - f(u_r)}{u_l - u_r} \qquad c = u_l u_r (u_l + u_r - 1) \ .$$

The wave speed is analogous to that given by the Rankine-Hugoniot condition (2.7). The numerical solution of (4.3) is obtained by imposing the asymptotic solutions at either side and breaking the translational invariance, see [1] for example. In this case we match the x co-ordinate for the position of the maximum film height. Of course since there may be some variation in this position

with different schemes, particularly for large h, we cannot do this exactly and must therefore choose a best fit.

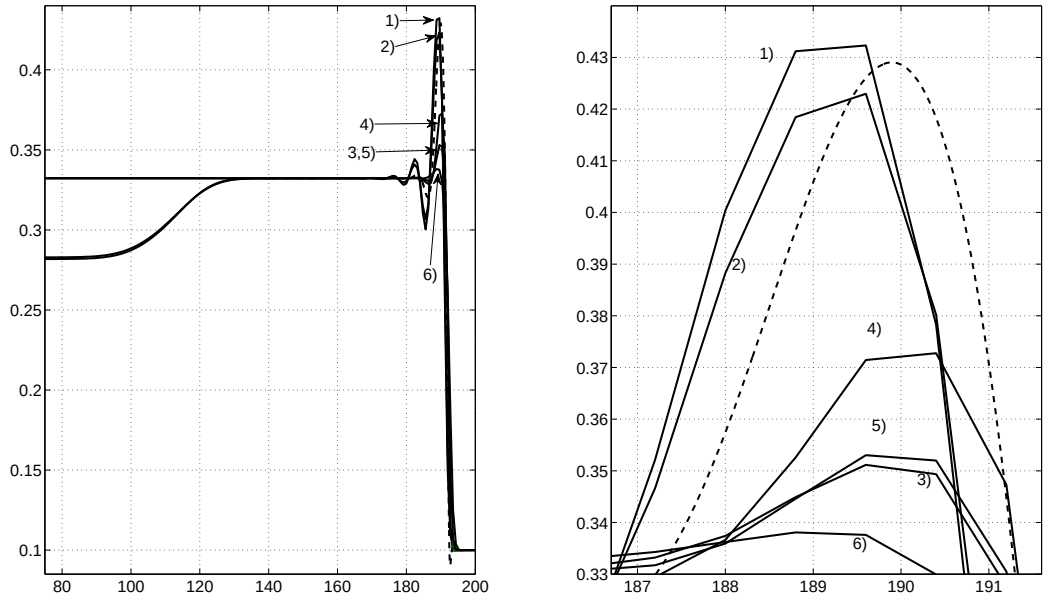

Fig. 3. Comparison of the numerical schemes with the travelling wave solution (4.3) with $u_l = 0.3323$, $u_r = 0.1$ for $h = 0.8$ at time $t = 500$. The curves are 1) CN, 2) FI, 3) WENO, 4) second-order Godunov, 5) CU, 6) first-order Godunov, and the travelling wave (dashed line).

In the following calculations we will assume that our numerical solution of equation (4.3) is the most accurate and therefore calculate errors based on this solution. In Figure 3 we compare results from the different numerical schemes with the solution of equation (4.3) (using the solution of equation (4.3) as the initial condition). The values $u_l = 0.3323$ and $u_r = 0.1$ are the same as those used in [3]. The figures show the film height around the moving front and a close-up of the peak. The step-size and time-step for the CN and FI schemes are $h = 0.8$, $\Delta t = 0.16$ (which gives a CFL number around 1/15). For the explicit methods we can take a larger time-step based on the CFL condition. In fact, we use a CFL of 0.75 for Godunov and CU, giving $\Delta t \approx 1.8$ and 0.5 for WENO, giving $\Delta t \approx 1.25$. On Figure 3a) it is difficult to distinguish between

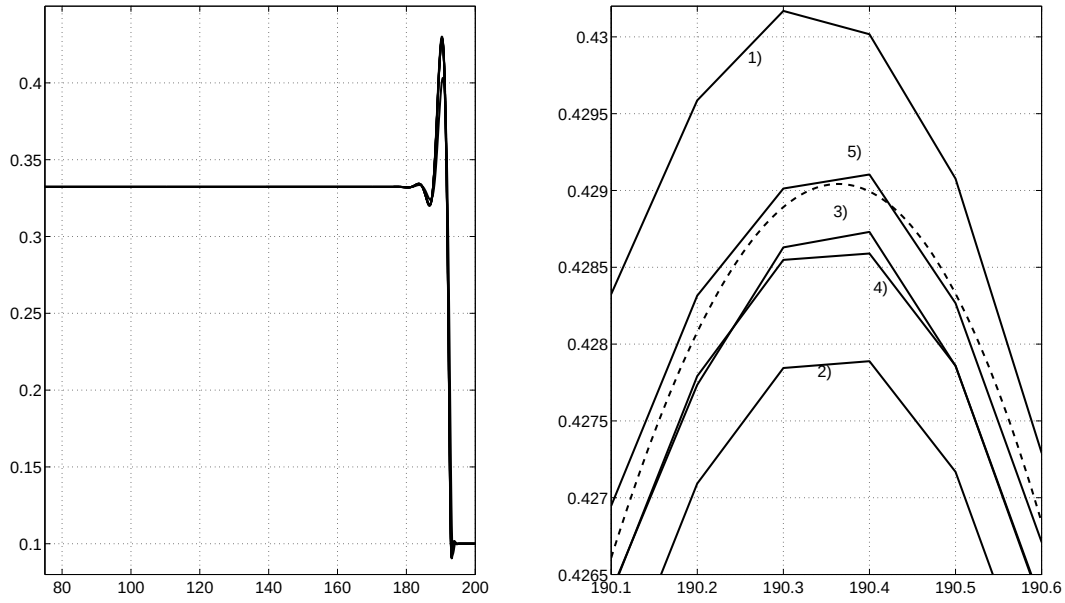

Fig. 4. Comparison of the numerical schemes with the travelling wave solution (4.3) with $u_l = 0.3323$, $u_r = 0.1$ for $h = 0.1$ at time $t = 500$. The curves are 1) CN, 2) FI, 3) WENO, 4) second-order Godunov, 5) CU and the travelling wave (dashed line).

the solutions. The distinction is clearer on Figure 3b). From this close-up it appears that the two implicit methods provide the best approximation to the travelling wave solution. However, these are the solutions on Figure 3a) that produce the large oscillations just downstream of the peak. It is also these two solutions that switch to a lower value for $x < 130$. This strange behaviour can be traced back to oscillations at small time which propagate backwards and act to reduce this left hand limit. Although the oscillations have moved out of the computational domain their effect on the film height remains. Note, the boundary condition at either end is $u_x = 0$. We will discuss this behaviour later in §4.2. The oscillations just downstream of the moving front, shown on Figure 3 a), come from the FI and CN solutions. From Figure 3 b) it is clear that the first order Godunov scheme provides the worst result. Decreasing the space-step allows the implicit schemes to approach the correct left hand limit and also acts to bring all the solutions closer to the travelling wave. This is

Method	h	0.8	0.4	0.2	0.1
First order Godunov	error	0.061472	0.0385403	0.0217701	0.0114021
	order	0.4696219	0.6735675	0.8240190	0.9330467
Second order Godunov	error	0.0269884	0.0073086	0.0012690	0.0000616
	order	1.3387111	1.8846742	2.5259018	4.3649633
WENO-LF	error	0.0408500	0.0115379	0.0020516	0.00010190
	order	1.0275280	1.8239518	2.4915681	4.33161454
Central-upwind	error	0.0497623	0.0144553	0.0017667	0.00016519
	order	0.7080527	1.7834557	3.0324377	3.41888707
Fully-Implicit	error	0.0026128	0.0056704	0.0019218	0.00049071
	order	2.2514125	-1.11784583	1.560980	1.96951699
Crank-Nicolson	error	0.0033870	0.00229690	0.0000532	0.0004732
	order	2.6960840	0.56030870	5.4322953	-3.1531860

Table 1
Comparison of errors and convergence orders for different schemes

shown on Figure 4, when $h = 0.1$ and $\Delta t = 0.02$ for the CN and FI schemes, $\Delta t \approx 0.225$ for Godunov and CU and $\Delta t \approx 0.156$ for WENO. On Figure 4 a) only the first order Godunov solution is distinguishable from the rest and this only in the vicinity of the peak. The close-up of Figure 4 b) does not capture the first-order Godunov solution. Near the peak it is now the explicit schemes that provide the best solution (with the exception of first-order Godunov). The two implicit schemes bound the explicit and travelling wave solutions.

In Table 1 we show the error and order of convergence for the different schemes. The error is defined as the absolute value of the difference between the maximum heights of the numerical and travelling wave solutions. The convergence order is defined in terms of the errors e_h and e_{2h}, corresponding to mesh widths h and $2h$,

$$|e_h| \sim 2^q |e_{2h}| \ .$$

Therefore, the convergence order is

$$q = \log_2(|e_{2h}|/|e_h|) \ .$$

The order in the first column in the table has been calculated using results for $h = 1.6$ (which are not shown). The explicit schemes show the expected convergence behaviour. First-order Godunov shows an approximately linear order of convergence, while the other three schemes appear to have a geometric convergence where, for example, the convergence order for $h = 0.1$ is much better than that of 0.2. The implicit schemes are more erratic. The FI scheme appears to have its best convergence order for $h = 0.8$, while CN appears best at $h = 0.2$ and shifts to a negative value for $h = 0.1$. It seems likely that this behaviour is related to our definition of convergence. When $h = 0.8$ the solution oscillates behind the peak, this may lead to a greater oscillation at the peak which is therefore higher than would occur without the oscillations. When $h = 0.4$ the oscillations are much reduced and the peak values decrease. Subsequent decreases in the step size result in the peak approaching the travelling wave peak in a more sensible manner. The explicit schemes, which do not suffer from the oscillatory behaviour, therefore converge as expected.

From now on we will use this travelling wave comparison to guide our choice of step-size or limiter. We will also neglect the first-order Godunov scheme, which is clearly significantly less accurate than the other schemes. In Figure 5 we show the effect of changing Δt with $h = 0.1$ on the CN scheme. The results of Figure 5 a) are indistinguishable. From the close-up of the peak, shown on Figure 5 b), we see that values of $\Delta t \in [0.01, 0.015]$ give a good approximation around the peak for this choice of h. Using similar comparisons we find the MC limiter and $\alpha = 1.35$ provide the best results for Godunov and CU schemes respectively. The WENO method appears to be robust with respect to changes

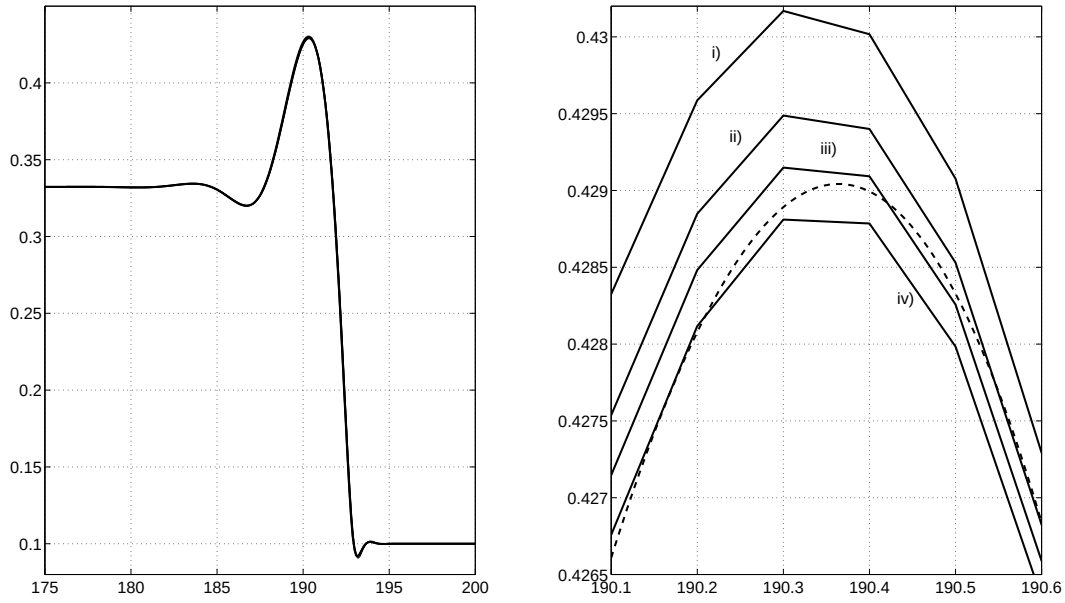

Fig. 5. The effect of changing Δt, for fixed $h = 0.1$, on the CN solution at time $t = 500$. The curves are i) $\Delta t = 0.02$, ii) 0.015, iii) 0.0125, iv) 0.01.

in the CFL number, with the solutions showing little variation for a CFL $\in [0.4, 0.6]$. We will discuss these choices in §4.3.

4.2 Effect of the moving grid substitution

We now consider the effect of adding the term $-su_x$ to the travelling wave of the previous section. If we take continuous initial data, such as that given in [3] then all solutions agree well, for sufficiently small space and time-step. However, when we start with discontinuous initial data, switching from u_l to u_r at $x = 0$ significant differences arise. Four sets of results for discontinuous initial data are shown on Figure 6. The first two, Figures 6 a), b), show solutions including the $-su_x$ term. The CN result is shown as a dashed line, the remaining solutions coincide, even to the level of the close-up of Figures 6 b), and are shown as the solid line. The final figures, Figures 6 c), d), show

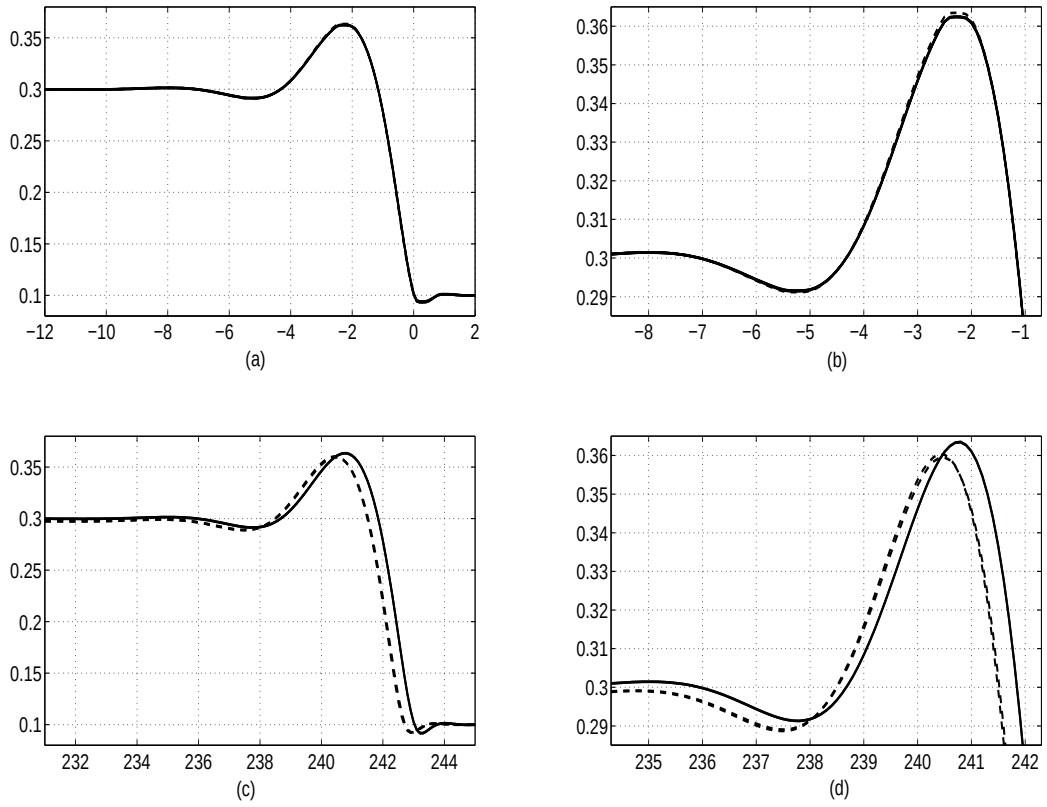

Fig. 6. Travelling wave with discontinuous initial data at t = 900, $h = 0.1$. Figures a), b) include $-su_x$ term.

results without the $-su_x$ term. The travelling wave and explicit schemes all coincide. As in Figure 3 a) the two implicit schemes, shown as dashed lines, tend to a lower left hand limit, although in the current situation the correct limit is never attained. Again this strange behaviour is a result of the initial oscillations caused by the discontinuity. This oscillation travels backwards and leads to the left hand limit slightly decreasing. The explicit schemes that avoid the oscillation do not suffer from this problem. In this case, the maximum wave height predicted by CN and FI schemes is also slightly lower and therefore slower than the explicit waves. If we begin with continuous data the results are all very similar to the explicit results for discontinuous data.

The change in behaviour between the figures is a result of the numerical scheme applied to the $-su_x$ term. The explicit schemes can all handle (and reduce) the oscillations that result from the application of the implicit diffusion term to discontinuous data. On the other hand the CN and FI terms propagate the oscillations. For consistency and to prevent the numerical treatment of the $-su_x$ term from affecting the results (somewhat erroneously as it now appears) we applied the central method to this term for all schemes. Like the tested explicit schemes, this method acts to reduce the oscillations and so improves the results for the implicit methods. Note, if we apply one of the other explicit schemes to this term it would also remove problem. If we use an implicit method to deal with the term then the problem remains.

This indicates a good reason to use the explicit schemes, which show consistent results regardless of the initial data. Further, the smaller time step of the implicit schemes means that they take more than twice the time required by the explicit schemes to produce a result.

4.3 Stable travelling waves?

Bertozzi *et al* [3] point out that for a range of far field heights, the system (1.1, 1.2) can support multiple shock profiles, but only two are stable. The first case they present uses a hyperbolic tangent initial profile with $u_l = 0.3323$, $u_r = 0.1$. The results are identical to those shown in our first example, in §4.1. The second stable wave involves an initial condition with a bump of width 10,

$$u(x) = \begin{cases} \frac{0.6-u_l}{2}\tanh(x+5) + \frac{0.6+u_l}{2} & \text{for } x < 0 \\ -\frac{0.6-u_r}{2}\tanh(x-5) + \frac{0.6+u_r}{2} & \text{for } x > 0 \ , \end{cases} \tag{4.4}$$

where $u_l = 0.3323$ and $u_r = 0.1$. Note, we have shifted the origin from that given in [3], since the governing equation is autonomous this will not affect the results. However, when the bump width is increased to 20, at large times the bump appears to spread out and so is classified as unstable.

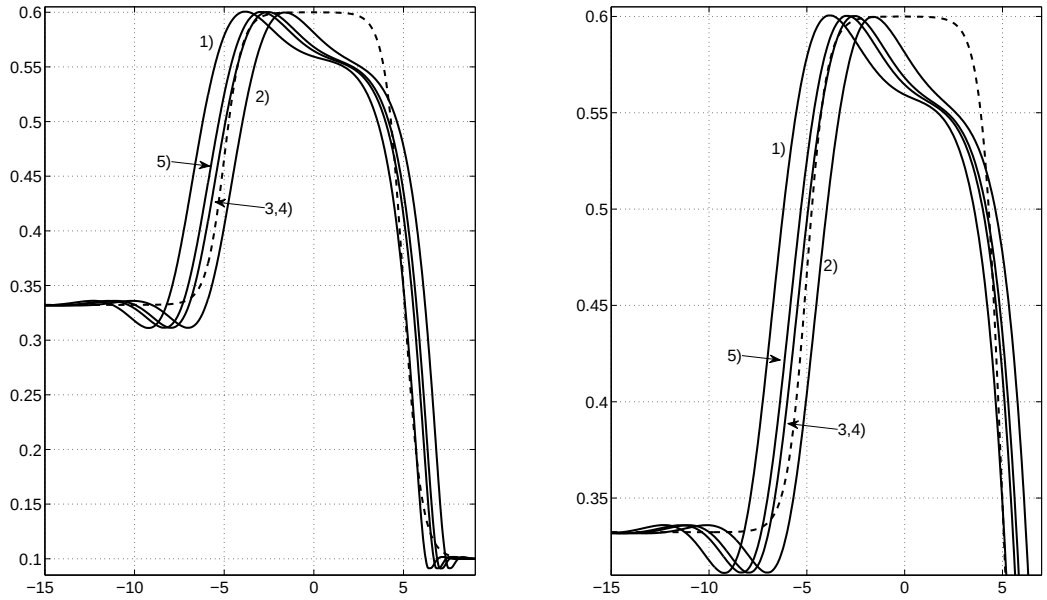

Fig. 7. The curves are 1) CN, 2) FI, 3) WENO, 4) second-order Godunov, 5) CU and the initial condition (dashed line), with $h = 0.05$.

In Figure 7 we present results for the initial profile of equation (4.4) at $t = 10^4$. In this case we solve the governing equation with a moving axis, given by equation (4.1). The Godunov and WENO results are hard to distinguish, so we have labelled them as a single curve. For the CN and FI schemes we take $\Delta t = 0.01$. For the explicit schemes we control the time-step with the CFL number, hence $\Delta t > 0.01$ and the explicit schemes are much faster than the implicit ones. All curves show that the initial hump changes to an undercompressive wave on the right and a compressive wave on the left. The bump width remains relatively constant for each scheme. This wave therefore appears stable.

Switching the initial condition, by replacing the 5 in equation (4.4) with a

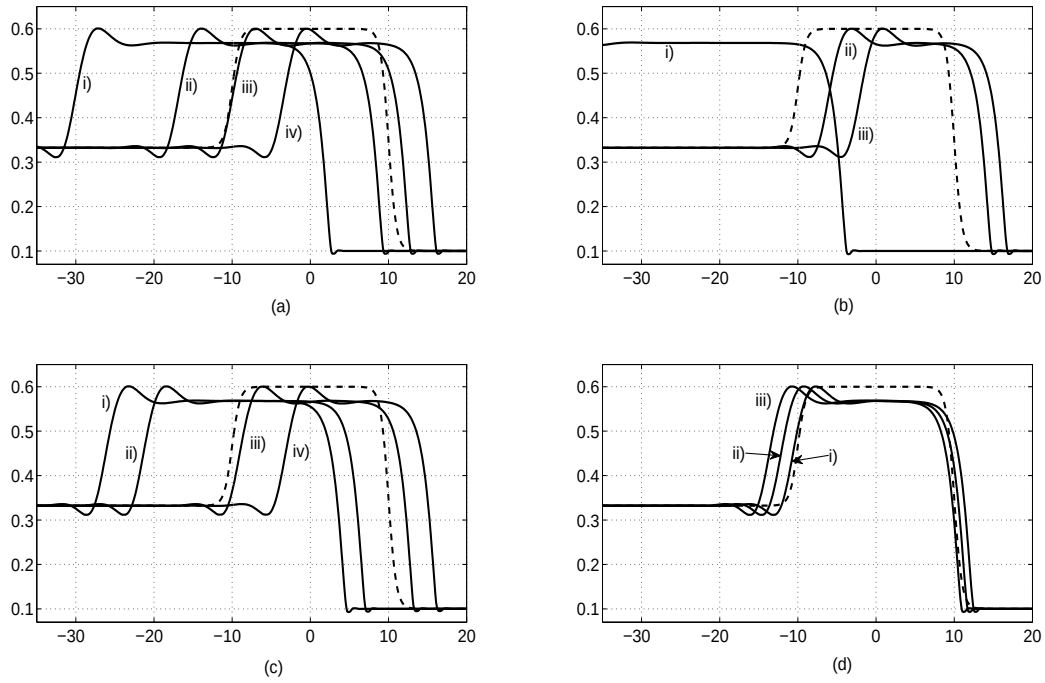

Fig. 8. Results at $t = 10^5$, with $h = 0.1$. The initial condition is a dashed line and a) CN, where $\Delta t =$ i) 0.02, ii) 0.015, iii) 0.0125, iv) 0.01, b) Godunov with i) SB, ii) VL, iii) MC, c) CU with i) $\alpha = 1.95$, ii) 1.5, iii) 1.25, iv) 1.2, d) WENO with CFL i) 0.4, ii) 0.5, iii) 0.6.

10, leads to the results for $t = 10^5$ shown in Figure 8. The FI scheme, which appears reasonable at $t = 10^4$ has moved out of the computational domain at 10^5 and so is not shown. In Figure 8 a) we see the effect of changing Δt on the evolution of the travelling wave using the CN scheme. When $\Delta t = 0.02$ the wave speed is less than that predicted by Rankine-Hugoniot. Further, the back and front ends of the wave move at a different speed resulting in the wave spreading out. This gives the appearance that the wave is unstable. Decreasing Δt does not necessarily fix the problem. With $\Delta t = 0.01$ the wave moves slightly too fast and also acts to reduce the width of the bump. In §4.1 we mentioned choosing Δt to give the least error compared to the travelling wave example of that section and suggested choosing $\Delta t \in [0.01, 0.015]$. From figure 8 a) we see when $\Delta t = 0.0125$ the downstream edge of the wave matches

the initial data. The upstream edge is slightly out, but of all cases this shows the least change in bump width. Similarly, with Godunov we found the MC limiter provided the best results and $\alpha \sim 1.35$ for CU. These are shown in Figures 8 c, d) respectively. WENO appeared relatively stable to changes in the CFL number. This is confirmed in Figure 8 d).

The results of Figure 8 indicate that this form of travelling wave is not unstable. It is merely the choice of numerical scheme and step sizes that lead to the bump spreading. In particular we note that WENO shows very little spread for a range of CFL numbers. The Godunov scheme appears sensitive to the choice of limiter. The SB limiter allows the bump to spread considerably, whereas MC and VL limiters maintain the initial width, with MC perhaps moving at the better speed. The CU scheme maintains the correct width when $\alpha \approx 1.25$ (slightly lower than the value 1.35 predicted earlier).

4.4 Double shock travelling wave

In our final example we examine the evolution of a double shock wave. This corresponds to Case 3 in [3]. In all cases we use the step sizes or limiters that have so far provided the best results. So far in this section, we have chosen examples where $u_l < 1/3$, which is where the flux has a point of inflexion. The following example shows the large effect that a small change in u_l can have. With continuous initial data all the schemes provide similar results. In Figure 9 we present solutions for the discontinuous initial data, $u = 0.4$ for $x < 0$, $u = 0.1$ for $x \geq 0$. Figures 9 a), b) show the solution near the travelling hump, including the $-su_x$ term and also a close up of the downstream edge of the hump. The FI solution is shown as the dotted line in Figure 9 a), the remaining curves are plotted as solid lines. In the close-up of Figure 9 b) we

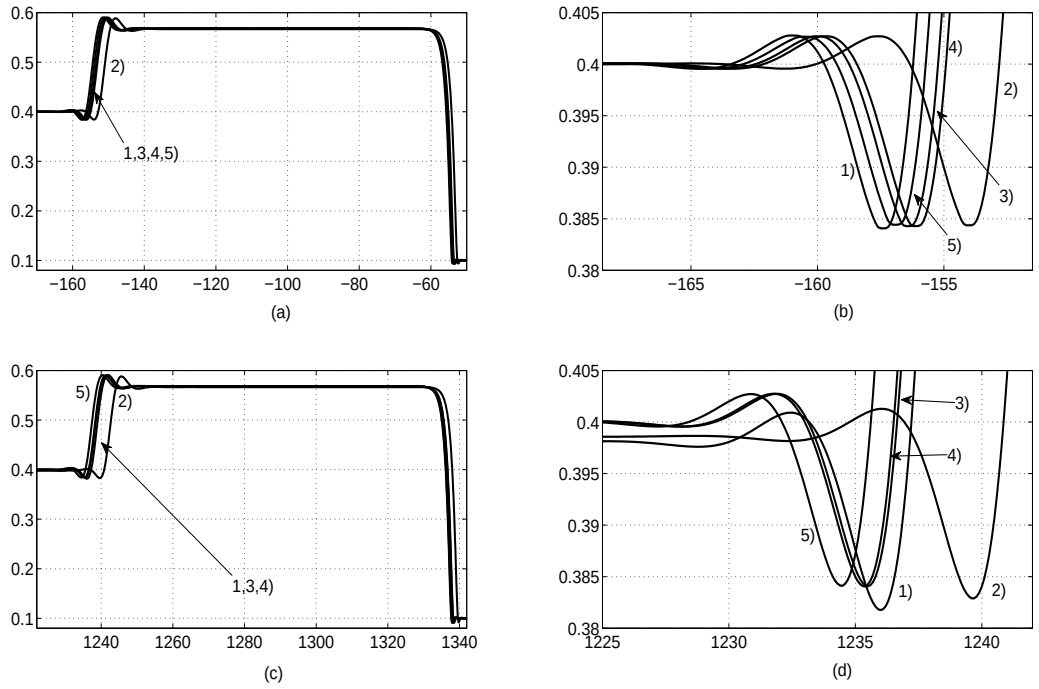

Fig. 9. Double shock with discontinuous initial condition at time = 4800 $h = 0.1$, $\Delta t = 0.02$ for CN and FI, The curves are 1) CN, 2) FI, 3) WENO, 4) second-order Godunov, 5) CU. Figures a), b) contain $-su_x$ term.

can see that the implicit schemes bound the implicit ones. Without the $-su_x$ term, as in previous examples we see that the implicit schemes tend to a lower left hand limit. The FI solution has also travelled further away from the other results.

5 Conclusion

We have presented a comparison of numerical schemes applied to a fourth-order thin film equation, with particular examples taken from the work of Bertozzi *et al* [3]. The results presented allow us to make a number of conclusions and recommendations regarding the numerical approximation of such schemes.

Firstly, we noted that applying a fractional step-splitting method provides much more stable results than when treating the convection and diffusion terms in a single step. If diffusion is neglected altogether, then all the methods considered dealt well with sufficiently continuous initial data. With discontinuous (on the scale of the space-step) initial data the implicit schemes all led to oscillations, while the explicit methods coped well. Of the explicit schemes WENO produced the least accurate result for the second discontinuous example.

When the fourth-order diffusion term is included it is clear that implicit methods should be applied to speed up calculations. We examined the effect of applying implicit schemes to the whole equation or combining an implicit diffusion scheme with an explicit convection term. The schemes that included an explicit step turned out to allow much larger time-steps and consequently significantly faster run-times. Further, the explicit results showed smaller errors and higher convergence order when compared to a standard travelling wave solution. Hence we conclude that the 'explicit' schemes are more computationally efficient and more accurate than the implicit ones.

When available the travelling wave solution can be used to determine appropriate values for time and space steps, limiters or the value of the CFL number. We carried this out in §4.1. For each method, except for CU where we were slightly out, our choice led to the best results in the example of §4.3. With the exception of WENO, the comparison in §4.3 highlighted the sensitivity of the methods to the limiter or time-step. WENO provided consistent and accurate results.

The use of discontinuous initial data led to surprising results. With the implicit schemes in particular, an oscillation at early time resulted in the large

time solution tending to an incorrect downstream limit. Possibly this could be fixed by specifying the limit value as a boundary condition, rather than using a zero derivative condition. However, it does highlight a possible problem with the implementation of the method. The explicit schemes all handled the discontinuity with no apparent problem. Note, as in the first example of §4.1 discontinuous can simply mean that changes occur over a smaller length-scale than the space-step. When the convective term $-su_x$ was included the problem with the implicit schemes was removed. This was a result of applying the central method to this term which gave the scheme a similar form to our other explicit schemes.

To summarize, from our calculations it appears that for the best accuracy and efficiency fourth-order diffusion equations with a convective term should be tackled using an explicit method on the convection term coupled to an implicit diffusion term by fractional step-splitting. The choice of explicit methods may be guided by a travelling wave solution. Our examples indicate that for this type of problem WENO is the most robust of the three methods investigated.

Acknowledgements

T.M. acknowledges the support of the Korean Advanced Institute of Science and Technology where this work was carried out. Y.J.K. was supported by the Korea Science and Engineering Foundation(KOSEF) grant funded by the Korea government(MOST) (No. R01-2007-000-11307-0).

References

[1] N. Balmforth, S. Ghadge and T.G. Myers, Surface tension driven fingering of a viscoplastic film, J. Non-Newtonian Fluid Mech. 142 (2007) 143-149.

[2] A. L. Bertozzi, M. P. Brenner, T. F. Dupont and L. P. Kadanoff, Singularities and similarities in interface flows in Trends and Perspectives in Applied Mathematics, Springer-Verlag, New York (1994) 155 -208.

[3] A.L. Bertozzi, A. Munch, M. Shearer, Undercompressive shocks in thin film flows, Physica D 134 (1999) 431-464.

[4] J.B. Greer, A.L. Bertozzi and G. Sapiro, Fourth order partial differential equations on general geometries, J. Comp. Phys. 216(1) (2006) 216–246.

[5] S. K. Godunov, Mat. Sbornik, **47** (1959) 271.

[6] Y. Ha, C. L. Gardner, A. Gelb and C.-W. Shu, Numerical Simulation of High Mach Number Astrophysical Jets with Radiative Cooling, J Sci. Comp. 24 (2005) 29–44.

[7] Y. Ha and Y.-J. Kim, Explicit solutions to a convection-reaction equation and defects of numerical schemes, J. Comput. Phys. 220 (1) (2006) 511-531.

[8] G.-S. Jiang, D. Levy, C.-T. Lin, S. Osher, and E. Tadmor, High-resolution non-oscillatory central schemes with non-staggered grids for hyperbolic conservation laws, SIAM J. Numer. Anal., 35 (1998) 2147–2168.

[9] G.-S. Jiang, C.-W. Shu, Efficient Implementation of Weighted ENO schemes, J. Comput. Phys. 126 (1) (1996) 202–228.

[10] D.E. Kataoka and S.M. Troian A theoretical study of instabilities at the advancing front of thermally driven coating films, J. Colloid & Interf. Sci. 192(2) (1997) 350–362.

[11] Y-J Kim Piecewise self-similar solutions and a numerical scheme for scalar conservation laws, SIAM J. Numer. Anal. 40(6) (2002) 2105–2132.

[12] J.S. Kim Adaptive mesh refinement for thin-film equations, J. Korean Phys. Soc. 49(5) (2006) 1903–1907.

[13] A. Kurganov, S. Noelle , and G. Petrova, Semi-discrete central-upwind schemes for hyperbolic conservation laws and Hamilton-Jacobi equations, SIAM J. Sci. Compu. 23 (2001) 707–740.

[14] A. Kurganov, and E. Tadmor, New high-resolution central schemes for nonlinear conservation laws and convection-diffusion equations, J. Comput. Phys. **160** (2000) 214–282.

[15] R.J. LeVeque, Numerical methods for conservation laws, Lectures in Mathematics ETH Zürich, Birkhäuser Verlag, Basel, 1990.

[16] R. J. LeVeque, High-resolution conservative algorithms for advection in incompressible flow. SIAM J. Numer. Anal. 33 (1996), 627–665

[17] R.J. LeVeque, Clawpack Version 4.3 Users Guide, University of Washington, Seattle, 2006. Available online at http://www.amath.washington.edu/∼claw/.

[18] X.-D. Liu, S. Osher, and T. Chan, Weighted essentially non-oscillatory schemes, J. Comput. Phys. **115** (1994) 200–212.

[19] T.G. Myers Thin films with high surface tension SIAM REV. 40(3) (1998) 441–462.

[20] T.G. Myers, J.P.F. Charpin and C.P. Thompson Slowly accreting ice due to supercooled water impacting on a cold surface, Phys. Fluids 14 (1) (2002) 240–256.

[21] T.G. Myers, J.P.F. Charpin, S.J. Chapman The flow and solidification of a thin fluid film on an arbitrary three-dimensional surface Phys. Fluids 14 (8) (2002) 2788-2803.

[22] H. Nessyahu and E. Tadmor, Non-oscillatory central differencing for hyperbolic conservation laws, J. Comput. Phys., 87 (1990), no. 2, 408–463.

[23] A. Oron, S.H. Davis and S.G. Bankoff Long-scale evolution of thin liquid films, Rev. Modern Phys. 69(3) (1997) 931–980.

[24] R.D. Russell, J.F. Williams, X. Xu MOVCOL4: A moving mesh code for fourth-order time-dependent partial differential equations SIAM J. Sci. Comp 29(1) (2007) 197–220.

[25] C.-W. Shu and S. Osher, Efficient implementation of essentially non-oscillatory shock capturing schemes, J. Comput. Phys. **77** (1988) 439–471.

[26] C.-W. Shu and S. Osher, Efficient implementation of essentially non-oscillatory shock capturing schemes, II, J. Comput. Phys. **83** (1989) 32–78.

[27] C.-W. Shu and S. Osher, Essentially non-oscillatory and weighted essentially non-oscillatory schemes for hyperbolic conservation laws, in Advanced Numerical Approximation of Nonlinear Hyperbolic Equations, B. Cockburn, C. Johnson, C.-W. Shu and E. Tadmor (Editor: A.Quarteroni), Lecture Notes in Mathematics, volume 1697, Springer, (1998) 325.

[28] E.F. Toro, Riemann Solvers and Numerical Methods for Fluid Dynamics : a practical introduction, Springer, 1999.

[29] B. van Leer, MUSCL, A New Approach to Numerical Gas Dynamics. In Computing in Plasma Physics and Astrophysics, Max-Planck-Institut fűr Plasma Physik, Garchung, Germany, April 1976.

[30] D. Vaynblat, J.R. Lister and T.P. Witelski Rupture of thin viscous films by van der Waals forces: Evolution and self-similarity Phys. Fluids 13(5) (2001) 1130–1140.